Central Power Research Institute

*Vol. 21(2)/117-125, December 2025*
*ISSN (Print) : 0973-0338*
*DOI : 10.33686/pwj.v21i2.1219*

*Power Research*

# Root Cause Analysis of SA213 T91 Superheater Tube of a Supercritical Power Plant

**D. Laxman Rao*** **and R. K. Kumar**

Materials Technology Division, Central Power Research Institute, Bengaluru - 560080, Karnataka, India; laxman@cpri.in

## Abstract

The premature failure of a SA213 T91 final superheater tube from an 800 MW supercritical coal-fired thermal power plant was investigated after 67,962 hours of service at high steam pressure (250 bar) and flue-gas temperatures of 800-970°C. The tube exhibited a longitudinal rupture accompanied by localised bulging, suggesting progressive deformation before failure. Although chemical analysis confirmed compliance with ASME SA213 T91 specifications, hardness reduction and loss of tensile strength were observed near the failed region. Microstructural examination revealed degradation of the tempered martensitic structure, characterised by carbide coarsening and preferential grain-boundary precipitation. Extensive grain-boundary cavitation and intergranular fracture features confirmed advanced creep damage. The failure was attributed to localised creep-induced microstructural and strength degradation during prolonged high-temperature exposure, resulting in tube rupture.

**Keywords:** Boiler Tube Failure, Creep Damage, Final Superheater Tube, High-temperature Service, SA213 T91 Steel, Supercritical

## 1. Introduction

Reducing carbon dioxide ($CO_2$) emissions from coal-based thermal power generation has become a critical requirement to address climate change and meet increasingly stringent environmental regulations worldwide. Studies have shown that improving the efficiency of fossil-fuel power plants through the adoption of Supercritical (SC) and Ultra-Supercritical (USC) technologies can significantly reduce $CO_2$, $SO_2$, and $NO_x$ emissions while enhancing overall plant performance[1-4]. The continuous improvement in thermal power plant efficiency has primarily been achieved by increasing main steam pressure and temperature, necessitating the development of advanced ferritic steels with superior creep strength capable of operating under supercritical conditions[5-8]. SA213 T91 steel is extensively used for superheater and reheater tubes in supercritical power plants because of its high creep strength derived from a tempered martensitic microstructure strengthened by MX carbonitrides and $M_{23}C_6$ carbides. However, long-term exposure to elevated temperatures leads to microstructural degradation through carbide coarsening and a loss of creep resistance, as widely reported for T91 steels in power plant applications. Ahmad et al. investigated the failure of a high-strength SA213 T91 superheater tube subjected to short-term overheating. Their analysis revealed the presence of creep cavities and microcracks, indicating severe high-temperature damage. Temperature estimation indicated that the tube had operated at temperatures exceeding 695°C, primarily due to uneven heat flux caused by inconsistent fuel feeding. The authors concluded that improper combustion was the root cause of the failure and emphasised that improved fuel management and regular internal inspections are essential to prevent similar failures[9]. Nurbanasari et al. investigated the failure of a secondary superheater tube in a 600 MW coal-fired power plant and concluded that the primary cause was the formation of slag deposits on the outer surface of the tube. These deposits led to localised flue-gas erosion and rapid overheating, resulting from the use of coal with an ash fusion temperature lower than the plant's design specifications. The failure analysis revealed a thin-lip rupture, reduced hardness, and

*Author for correspondence

© Power Research

the presence of coarse carbides, which are consistent with overheating and creep-related damage[10]. Kumar *et al.*[11] conducted a failure analysis of a T91-grade reheater tube in a supercritical power plant. They identified prolonged overheating and microstructural degradation, including creep cavitation and oxidation, as the primary causes of failure. Their study further highlighted the combined influence of elevated operating temperatures and residual stresses introduced during tube bending on the component's premature failure[12]. Arvind Kumar et al. analysed failures of T91 boiler tubes in a thermal power plant and reported that the failures were primarily associated with short-term overheating. Their microstructural analysis revealed features characteristic of thermal damage, indicating that overheating was the dominant cause of tube degradation and failure[11]. Zhang *et al.*[13] investigated cracking and leakage in T91 steel tubes of a supercritical boiler and found that manufacturing-induced internal linear defects acted as stress concentrators, promoting crack initiation and propagation during hydraulic testing. Their study emphasised the need for improved nondestructive testing techniques to detect such defects and prevent premature tube failures. Munif et al. investigated the failure of T91 superheater tubes in a 600 MW coal-fired power plant and identified two dominant failure modes: creep-induced thick-lip rupture under prolonged high-temperature exposure and thin-lip fish-mouth rupture caused by erosion-corrosion associated with ash deposition. Their study highlighted the combined influence of elevated operating temperature and deposit accumulation on tube degradation and emphasised the importance of periodic deposit removal to enhance service life of boiler tubes[14].

## 2. Operational Conditions

A boiler tube sample from an 800 MW supercritical coal-fired thermal power plant was investigated following a failure in the Final Superheater (FSH) section, approximately 67,962 h of service. The failure occurred at an elevation of about 65 m. The tube was manufactured from SA213 T91 grade steel with a nominal outer diameter of 44.45 mm and a wall thickness of 7.11 mm. During operation, the tube was exposed to flue-gas temperatures of 800-970°C, a steam pressure of approximately 255 bar, and a steam temperature of 568°C. The unit had experienced fifty-eight shutdowns since commissioning, and the failure was reported for the first time at this location.

## 3. Methodology

Failed and unfailed superheater tube samples were examined to determine the cause of failure. Visual and dimensional examinations were performed to evaluate macroscopic deformation, rupture characteristics, and localised bulging. Chemical composition of the tube material was determined using Optical Emission Spectroscopy (OES). Hardness and wall thickness measurements were performed along the tube length to assess localised material softening. Tensile tests were conducted on specimens extracted from failed and unfailed tubes in accordance with ASTM E8. Microstructural characterisation was performed using optical microscopy and scanning electron microscopy (SEM) with Energy-Dispersive X-ray Spectroscopy (EDS) to examine microstructural degradation, precipitate characteristics, and fracture features.

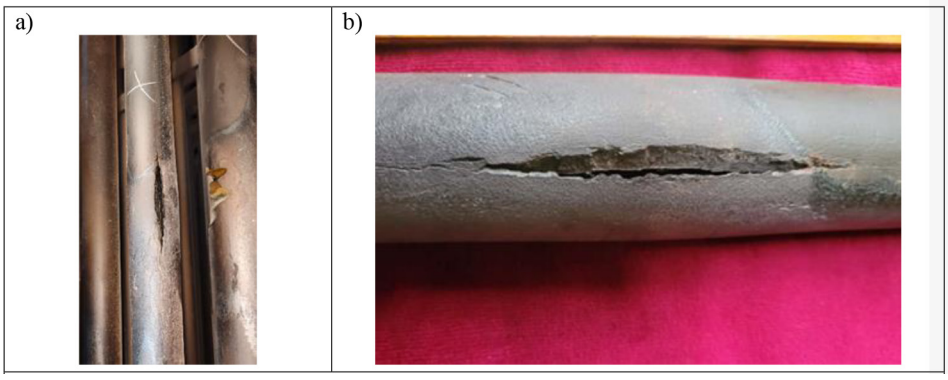



**Figure 1.** **(a)** Site photograph showing longitudinal rupture of tube inside the boiler; **(b)** close-up view of the tube showing thick-lip opening and localised bulging near the rupture region.

# 4. Results and Discussion

## 4.1 Visual Examination

The boiler tube sample from the final superheater section exhibited localised failure. The site photograph of the failed tube inside the boiler is shown in Figure 1(a), where a longitudinal rupture is clearly visible along the tube length. The damage was confined to a localised region, with areas away from the rupture opening showing no significant degradation. A close-up view of the removed tube segment is presented in Figure 1(b). The tube exhibited a longitudinal slit opening accompanied by localised bulging at the rupture mouth, indicating significant plastic deformation prior to rupture. The edges of the opening appeared thick and rounded, which is characteristic of a thick-lip rupture morphology typically associated with creep damage in boiler tubes subjected to prolonged high-temperature service. No evidence of sharp, brittle fracture features was observed at the macroscopic level.

## 4.2 Chemical Composition

The chemical composition of the failed superheater tube was determined using an optical emission spectrometer (ARUN Technology, Model PolySpek Neo). The analysis was carried out at multiple locations along the tube to ensure compositional consistency, and the average elemental concentrations (wt. %) are presented in Table 1. For comparison, the composition of a virgin SA213 T91 tube is also included. The results indicate that the chemical composition of the failed tube meets the specified limits for SA213 T91 steel.

## 4.3 Hardness Measurement

Hardness measurements were performed on the failed superheater tube to evaluate localised material degradation and were compared with those of a virgin tube. Measurements were carried out using a portable hardness tester (Make: Accuplus, Model: TH110A). The locations of hardness measurements along the failed superheater tube are shown in Figure 2, and the corresponding hardness values recorded at the front and back regions are presented in Table 2. The virgin tube exhibited a hardness of 190-205 BHN, whereas the failed tube showed significantly lower hardness. Away from the rupture region, hardness values ranged between 140 and 170 BHN, while pronounced softening was observed near the rupture region, where hardness decreased to approximately 120-130 BHN in the front region. The reduction in hardness indicates localised material softening associated with prolonged high-temperature exposure and creep.

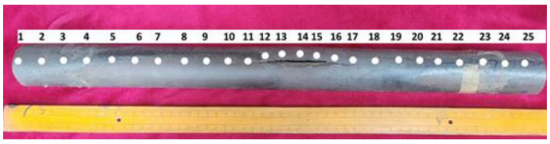



**Figure 2.** Photograph of the failed superheater tube showing locations of 25 hardness and thickness measurements; readings 12-19 correspond to the rupture-affected region.

## 4.4 Wall Thickness Measurement

Wall thickness measurements were conducted on the failed superheater tube to assess localised thinning using an Olympus Model 38DLPlus ultrasonic thickness gage. The measured thickness values along the failed tube are presented in Table 3. The virgin tube had a nominal wall thickness of 7.45-7.60 mm. The failed tube retained a thickness of approximately 6.5-7.1 mm in regions away from the rupture. However, localised thinning was observed near the bulged region, where the thickness has decreased to 5.56-6.13 mm. In addition, the tube exhibited localised bulging near the rupture region, with the outer diameter increasing from about 46 to 48 mm, corresponding to an estimated bulge of 3-4%. The reduction in wall thickness, combined with localised bulging, suggests material degradation associated with long-term high-temperature service and creep deformation.

**Table 1.** Chemical composition of failed and virgin superheater tubes compared with ASME SA213 T91 specification limits (wt. %)

| Tube details | C | Mn | Si | Cr | Mo | Ni | V | P | S |
|---|---|---|---|---|---|---|---|---|---|
| Failed SH tube | 0.10 | 0.52 | 0.36 | 8.45 | 0.92 | 0.20 | 0.24 | 0.014 | 0.009 |
| Virgin T91 tube | 0.11 | 0.58 | 0.34 | 8.77 | 0.93 | 0.16 | 0.25 | 0.013 | 0.010 |
| ASME SA213 T91 | 0.08 to 0.12 | 0.3 to 0.60 | 0.2 to 0.50 | 8.00 to 9.50 | 0.85 to 1.05 | ≤0.40 | 0.18 to 0.25 | ≤0.020 | ≤0.010 |

**Table 2.** Hardness measurements along the failed superheater tube

| Location No. | Hardness (BHN) | Reading No. | Hardness (BHN) |
|---|---|---|---|
| 1 | 150 | 14 | 125 |
| 2 | 145 | 15 | 120 |
| 3 | 148 | 16 | 124 |
| 4 | 142 | 17 | 122 |
| 5 | 140 | 18 | 126 |
| 6 | 138 | 19 | 129 |
| 7 | 136 | 20 | 138 |
| 8 | 144 | 21 | 140 |
| 9 | 152 | 22 | 145 |
| 10 | 146 | 23 | 150 |
| 11 | 142 | 24 | 148 |
| 12 | 130 | 25 | 152 |
| 13 | 128 | | |

**Table 3.** Wall thickness measurements along the failed superheater tube

| Location No. | Thickness (mm) | Reading No. | Thickness (mm) |
|---|---|---|---|
| 1 | 7.10 | 14 | 5.89 |
| 2 | 7.05 | 15 | 6.01 |
| 3 | 6.91 | 16 | 6.13 |
| 4 | 6.84 | 17 | 5.72 |
| 5 | 6.72 | 18 | 5.91 |
| 6 | 6.89 | 19 | 5.93 |
| 7 | 6.81 | 20 | 6.87 |
| 8 | 6.59 | 21 | 6.94 |
| 9 | 6.67 | 22 | 6.82 |
| 10 | 6.69 | 23 | 6.97 |
| 11 | 6.54 | 24 | 7.12 |
| 12 | 5.56 | 25 | 7.08 |
| 13 | 5.71 | | |

## 4.4 Mechanical Properties Evaluation

Tensile tests were performed on specimens extracted from the failed superheater tube at locations near the failure region and 150 mm away, and the results were compared with those of a virgin SA213 T91 tube. The specimen extraction locations are shown in Figure 3. All tensile specimens were prepared and tested in accordance with ASTM E8 standards, and the resulting mechanical properties are summarised in Table 4. The virgin tube exhibited a yield strength of 512 MPa, an ultimate tensile strength of 710 MPa, and an elongation of about 17%, indicating higher strength with comparatively lower ductility than the minimum ASME SA213 T91 requirements. The lower ductility appears to be due to minor variations in heat treatment and to a strongly tempered martensitic microstructure with fine carbides. In contrast, the failed tube specimens showed a significant reduction in strength. The specimen extracted near the rupture exhibited a yield strength of 317 MPa and an ultimate tensile strength of 527 MPa, accompanied by a higher elongation of 25.3%, indicating pronounced strength degradation with retained ductility due to prolonged high-temperature exposure. The specimen away from the failure showed similar degraded strength levels, with a yield strength of 295 MPa, a tensile strength of 500 MPa, and an elongation of 21.97%. The observed mechanical properties of the tube confirm localised material degradation under service conditions, consistent with creep-induced damage.

**Table 4.** Mechanical properties of failed and virgin SA213 T91 superheater tubes compared with specification requirements

| Tube description | Yield strength (MPa) | Ultimate tensile strength (MPa) | Elongation (%) |
|---|---|---|---|
| Failed tube - near failure | 317 | 527 | 25.30 |
| Failed tube -away from failure | 295 | 500 | 21.97 |
| Virgin tube | 512 | 710 | 17.00 |
| ASME SA213 T91 (min.) | ≥415 | ≥585 | ≥20 |




**Figure 3.** Location of tensile test specimens extracted from the Superheater tube for mechanical property evaluation.

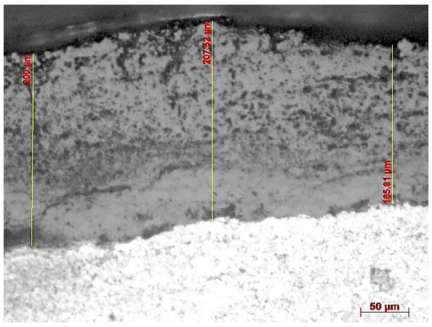



**Figure 4.** Optical micrograph showing the ID side coating thickness of the final superheater tube near the failed region

## 4.5 Microstructure Analysis

The metallurgical condition of the superheater tube was evaluated through optical microstructural examination. Specimens were extracted from the failed tube near the rupture region and from a virgin SA213 T91 tube for comparison. The samples were prepared using standard metallographic techniques and etched with a solution of 90 ml ethyl alcohol, 5 g $FeCl_3$, and 10 ml HCl (37% conc.) to reveal the microstructural features. Microstructural observations were carried out using a Carl Zeiss Axio Imager A2 optical microscope. The virgin tube exhibited a typical tempered martensitic microstructure consisting of fine lath structures with uniformly distributed fine carbides along lath and sub-grain boundaries (Figure 4). Such a microstructure is characteristic of T91 steel and is responsible for its high creep strength and thermal stability during high-temperature service. In contrast, the failed tube specimens showed pronounced microstructural degradation. The microstructure near the rupture region (Figure 5) revealed significant carbide coarsening with preferential precipitation along prior-austenite grain boundaries and martensitic lath boundaries. The observed carbide coarsening and loss of uniform precipitate distribution indicate microstructural instability during prolonged high-temperature exposure, resulting in reduced creep resistance. In addition, the oxide scale thickness on the Inner Diameter (ID) side of the final superheater tube near the failed region was examined. The observed cross-sectional micrograph is shown in Figure 6. The measurements were taken around the failed opening region. The observed oxide scale thickness ranged from 165 to 210 µm, suggesting significant high-temperature oxidation during service.

The oxide growth in T91 steels follows parabolic kinetics, which provides the growth of oxide scale under diffusion-controlled conditions. The parabolic rate constant is determined using the formula

$$x^2 = k_p . t$$

where, x = oxide thickness (µm)

$k_p$ = pararablic constant (µm²/h)

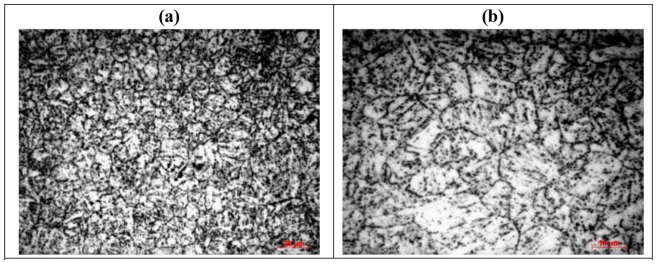



**Figure 5.** Optical micrographs of virgin SA213 T91 tube showing a tempered martensitic structure with fine, uniformly dispersed carbides: **(a)** 200X magnification; **(b)** 500X magnification.

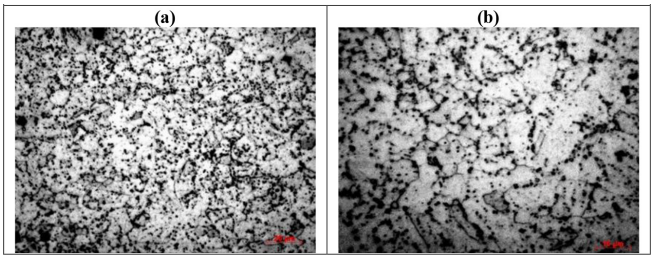



**Figure 6.** Optical micrographs of the failed superheater tube near the rupture region showing coarsened carbides and preferential grain-boundary precipitation: **(a)** 200X magnification; **(b)** 500X magnification.

t = time ( h)

For the observed oxide thickness of 220µ after 48000 hrs of service (70% of the service period), the calculated kp value amounts to 1.0083 µm²/h. Based on reported oxidation kinetics of T91 steels, the temperature dependence of the parabolic rate constant can be expressed using the following empirical Arrhenius-type relationship[15].

$Log_{10} (k_p) = 12.552 - 10784 / T$

where, $k_p$ = µm²/h

T = Temp of tube metal, Kelvin

For a 220 µm thick layer, the calculated kp value is 1.0083 µm²/h, and the estimated service temperature is 586°C. Thus, the estimated tube metal temperature was 586°C, which is higher than the design value by 46°C. This would result in a gradual increase in oxide growth and early-stage creep damage.

## 4.6 SEM Examination

Scanning Electron Microscopy (SEM) analysis was performed to examine microstructural degradation in the failed superheater tube and to compare it with that of a virgin SA213 T91 tube. SEM observations were carried out using a scanning electron microscope (Make: Carl Zeiss, Model: EVO 18). The virgin tube exhibited a relatively homogeneous ferritic-martensitic matrix with uniformly distributed fine precipitates and no evidence of voids or microcracks, as shown in Figure 7. SEM examination of the failed tube near the rupture region revealed clear evidence of creep-related damage. Multiple creep voids and cavities were observed predominantly along grain boundaries, as shown in Figure 8(a-d). In several locations, these voids were found to coalesce, forming microcracks along grain boundaries. The presence of cavity linkage and crack networks is characteristic of advanced creep damage, indicating prolonged exposure to elevated temperature and stress during service. The SEM observations provide strong evidence that creep-induced microstructural degradation played a dominant role in the superheater tube's failure.

## 4.7 Fracture Surface Examination

Fracture-surface examination of the failed superheater tube was conducted to determine the mode of failure. The fracture surface, as shown in Figure 9, exhibited predominantly intergranular features. The fracture surface was characterised by grain-boundary facets and interconnected cavities, indicating the nucleation and subsequent coalescence of creep cavities along grain boundaries. Such intergranular fracture morphology is characteristic of creep-induced embrittlement in ferritic-martensitic steels, where prolonged high-temperature exposure promotes carbide coarsening and grain-boundary weakening, ultimately leading to rupture.

## 4.8 SEM and EDS Analysis of Precipitates

SEM-EDS analysis was performed to characterise the chemical composition of the coarse precipitates observed in the failed superheater tube. Point EDS analyses (Free Draw 1-3) were performed on the coarse precipitates, while selected area analyses (Selected Area 1 and 2) were conducted on the surrounding matrix regions, as indicated in Figure 10. The quantitative elemental compositions obtained from these analyses are summarised in Table 5. The EDS results show that the coarse precipitates are significantly enriched in chromium, with concentrations ranging from approximately 18 to 38 wt.%, compared to about 7-8 wt.%

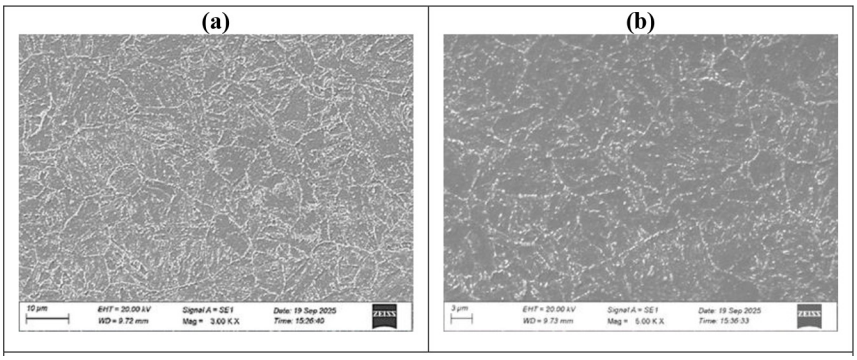



**Figure 7.** SEM micrographs of the virgin SA213 T91 tube showing a finely distributed precipitate and absence of creep voids or cracks: (a) 3,000X; (b) 5,000X magnification.

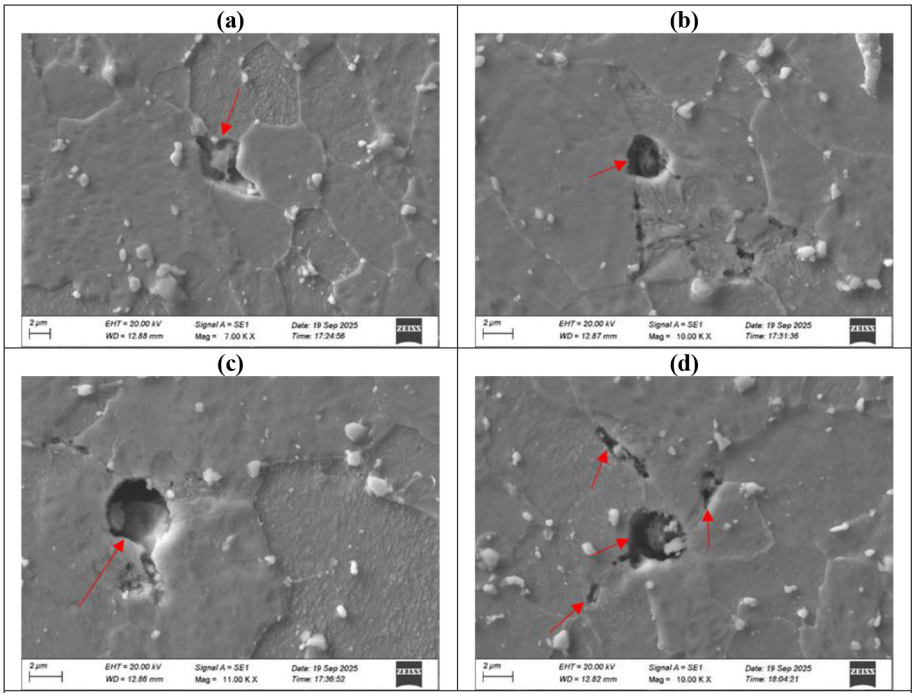



**Figure 8.** SEM micrographs of the failed superheater tube near the rupture region showing creep-related damage: **(a)** grain-boundary creep voids and cavities at 7000X magnification; **(b-d)** grain-boundary cavitation with void coalescence and microcrack formation at 10,000X.

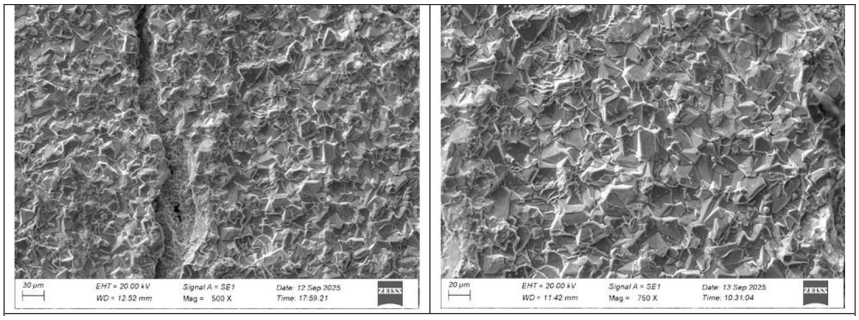


**Figure 9.** SEM fractographs of the failed superheater tube showing intergranular fracture with creep cavity coalescence and grain-boundary crack linkage.

chromium in the matrix regions. Carbon content in the precipitates was also markedly higher (~6-9 wt.%) than in the matrix (~2-3 wt.%). In addition, molybdenum enrichment was observed in the precipitates, with values of 3-6 wt.%, whereas the matrix contained 1-1.5 wt.% molybdenum. The pronounced enrichment of Cr, C, and Mo in the coarse precipitates confirms that these phases are chromium-rich carbides formed during long-term high-temperature service. The compositional contrast between the precipitates and the matrix indicates significant redistribution of alloying elements, consistent with microstructural degradation associated with prolonged exposure to elevated temperatures.

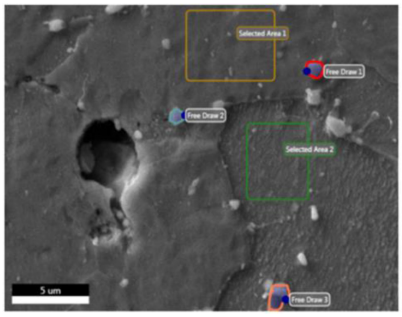



**Figure 10.** SEM micrograph of the failed tube showing locations selected for EDS analysis: point analyses on coarse precipitates (Free Draw 1-3) and selected area analyses on the surrounding matrix (Selected Area 1 and 2).

**Table 5.** SEM-EDS elemental composition (wt%) of coarse precipitates and matrix regions in the failed superheater tube

| Area | Carbon | Silicon | Molybdenum | Chromium | Vanadium | Manganese | Iron |
|---|---|---|---|---|---|---|---|
| Free Draw 1 | 6.89 | 0.45 | 5.51 | 37.76 | 0.30 | 0.50 | 48.59 |
| Free Draw 2 | 8.67 | 0.56 | 3.59 | 18.12 | 1.55 | 1.28 | 66.22 |
| Free Draw 3 | 6.45 | 0.46 | 3.70 | 22.91 | 0.34 | 0.22 | 65.93 |
| Area 1 | 2.57 | 0.37 | 1.25 | 7.07 | 0.07 | 0.29 | 88.36 |
| Area 2 | 2.29 | 0.26 | 1.17 | 7.32 | 0.11 | 0.22 | 88.64 |

## 5. Discussion

The macroscopic features, including longitudinal rupture with localised bulging and a thick-lip opening, indicate progressive deformation prior to failure, which is characteristic of creep-dominated rupture in high-temperature boiler tubes. Hardness measurements revealed severe localised degradation near the rupture region, with hardness reducing to approximately 120-130 BHN, and the associated localised bulging further confirms creep-induced deformation under sustained internal steam pressure. Tensile testing showed significant strength degradation in specimens taken from a failed superheater tube, indicating loss of creep strength. Optical and SEM microstructural examinations revealed pronounced degradation of the tempered martensitic structure, characterised by extensive carbide coarsening and preferential precipitation along grain and lath boundaries. Such microstructural instability in T91 steels during long-term service is known to reduce grain-boundary strength and accelerate creep deformation[16-18]. SEM-EDS analysis further indicated significant enrichment of chromium, carbon, and molybdenum in coarse precipitates, consistent with the formation and growth of chromium-rich carbides during prolonged high-temperature exposure. Fracture surface examination revealed predominantly intergranular fracture, with evidence of creep-cavity coalescence and grain-boundary crack linkage, confirming creep-induced embrittlement as the dominant failure mode.

## 6. Conclusions

The failure of the SA213 T91 final superheater tube was caused by creep under prolonged high-temperature service. Localised bulging, reduced hardness, and a significant loss of tensile strength near the rupture region indicate progressive degradation. Microstructural instability, evidenced by carbide coarsening and grain-boundary cavitation confirmed by SEM and EDS analyses, led to creep-induced embrittlement and intergranular fracture. Such degradation is characteristic of creep-dominated damage in ferritic-martensitic steels, where long-term thermal exposure promotes precipitate coarsening and grain-boundary weakening. The combined macroscopic, mechanical and microstructural evidence demonstrates that long-term exposure to elevated temperature and stress resulted in progressive creep damage and ultimate longitudinal rupture of the tube.

## 7. Acknowledgement

The authors acknowledge the Central Power Research Institute (CPRI), Bangalore, for its continuous support in conducting this study.

## 8. References

1. Tan X. Supercritical and ultrasupercritical coal-fired power generation. J Washington Instit China Stud. 2012; 6(1):53-72.
2. Bhiogade DS. Ultra supercritical thermal power plant material advancements : A review. J Alloy Metall Syst. 2023; 3:100024. https://doi.org/10.1016/j.jalmes.2023.100024
3. Tramošljika B, Blecich P, Bonefačić I, Glažar V. Advanced ultra-supercritical coal-fired power plant with post-combustion carbon capture : Analysis of electricity penalty and $CO_2$ emission reduction. Sustainability. 2021; 13(2):801. https://doi.org/10.3390/su13020801
4. Kumar D, Kumar D. Chapter 2 - Coal usage and control of $CO_2$ emissions. Sustainable management of coal preparation, Woodhead Publishing; 2018. p. 15-33. https://doi.org/https://doi.org/10.1016/B978-0-12-812632-5.00002-1
5. Mayer K-H, Masuyama F. The development of creep-resistant steels. 2-The development of creep-resistant steels. Creep-Resistant Steels; 2008. p. 15-77. https://doi.org/10.1533/9781845694012.1.15

6. Abe F. 1 – Introduction. Creep-Resistant Steels, Woodhead Publishing Series in Metals and Surface Engineering; 2008: p. 3-14. https://doi.org/https://doi.org/10.1533/9781845694012.1.3
7. Ennis PJ, Czyrska-Filemonowicz A. Recent advances in creep-resistant steels for power plant applications. Sadhana. 2003; 28(3-4):709-730. https://doi.org/10.1007/BF02706455
8. Abe F. 9 - Development of creep-resistant steels and alloys for use in power plants. Structural alloys for power plants operational: Challenges and high-temperature materials, Woodhead Publishing Series in Energy; 2014. p. 250-293. https://doi.org/https://doi.org/10.1533/9780857097552.2.250
9. Ahmad J, Purbolaksono J, Beng L, Ahmad A. Failure evaluation on a high-strength alloy SA213-T91 super heater tube of a power generation. Proc Inst Mech Eng, Part E: J Proc Mech Eng. 2010; 224:269-273. https://doi.org/10.1243/09544089JPME332
10. Nurbanasari M, Abdurrachim H, Prihadi MM. Failure analysis of secondary superheater tube in a 600-MW. J Fail Anal Prev. 2019; 19:453-460. https://doi.org/10.1007/s11668-019-00619-9
11. Kumar A, Roy M, Janardhana M, Kumar MS. Failure analysis of high strength T91 boiler tubes used in thermal power plant : A case study. Pow Res. 2016; 12(2):363-370.
12. A. Varma, F.A. Group, G. Noida, failure analysis of t91 grade reheater tube of a. 2018:651-655.
13. Zhang Y, Zhang X, Zhang Z, Gong Y. Cause analysis of cracking and leakage of T91 steel tube in hydraulic test of supercritical boiler. IOP Conf Ser: Earth Environ Sci. 2020; 512:012177. https://doi.org/10.1088/1755-1315/512/1/012177
14. Plant P, Munif KA. Failure analysis of superheater tubes made from material T91 in the Boiler of a 600 MW Power Plant. Int J Mech Eng Sci. 2020; 4(1):24-32. https://doi.org/10.12962/j25807471.v4i1.6421
15. Laverde D. Continuous and cyclic oxidation of T91 ferritic steel under steam. Corros Sci. 2004; 46(3):613-631. https://doi.org/10.1016/S0010-938X(03)00173-2
16. Zheng Q, Zhong W, Bai B, Yang W, Wang Z, Huang C. Research on the Fracture Behavior and Microstructure of T91 Steel at Ultrahigh Creep Temperatures. 2022; 12(12):2054. https://doi.org/10.3390/met12122054
17. Li Y, Du J, Li L, Gao K, Pang X, Volinsky AA. Mechanical properties and phases evolution in T91 steel during long-term high-temperature exposure. Eng Fail Anal. 2020;111:104451. https://doi.org/10.1016/j.engfailanal.2020.104451
18. Lok V, Le TG, Yu JM, Ma YW, Nguyen VP. Changes in creep property and precipitates due to aging of T91 steel after long-term service. J Mech Sci Technol. 2020; 34:3283-3293. https://doi.org/10.1007/s12206-020-0720-4Bottom of Form